Numerical Analysis and Experimental Characterization of Brick Masonry

Jamiu A. Dauda*

School of Civil Engineering,
University of Leeds, LS2 9JT Leeds, United Kingdom.
Email: cnjad@leeds.ac.uk
*Corresponding author

Ornella Iuorio

School of Civil Engineering,
University of Leeds, LS2 9JT Leeds, United Kingdom.
Email: o.iuorio@leeds.ac.uk

Paulo B. Lourenco

ISISE, Department of Civil Engineering,
University of Minho, Campus de Azurem, 4800-58, Guimarães, Portugal
Email: pbl@civil.uminho.pt

Abstract: Simulating the mechanical behaviour of masonry structures by using numerical analysis is still a complex subject because the process is hindered by little knowledge of the properties of masonry constituents and the interface. In particular, the definition of mechanical properties of masonry components is a key issue when finite element analysis is adopted for the prediction of the mechanical behaviour of masonry walls under accidental and exceptional loads. In an attempt to develop a detailed micro-modelling of brick masonry under compression, where the brick unit, mortar and brick-mortar interface are defined by their corresponding mechanical properties obtained through experimental testing, this work presents experimental tests on brick units, mortar and small masonry cubic specimens. Hence, a detailed micro-modelling of brick masonry cubic specimen is developed in ABAQUS. The numerical model is calibrated and validated based on the results obtained from the experimental tests on masonry cubic specimens. The results show that the numerical model is able to predict the mechanical behaviour of the masonry specimen with a 95% accuracy in terms of compressive strength.

Biographical notes: Jamiu A. Dauda has master degree in structural engineering and he is presently a doctoral research student within the School of Civil Engineering, University of Leeds, UK. Jamiu's present research proposed an investigation into the possibility of retrofitting unreinforced masonry (URM) wall using timber-panel. This project is part of the wider scope ''Retrofit of

Historical Structures''.

Ornella Iuorio is an assistant professor in school of civil engineering at the University of Leeds. She is a researcher and designer interested in innovation and interdisciplinary collaboration between architecture, structural engineering and environment. Ornella's research is in the field of retrofit of historical neighbourhoods, light weight steel structures and free from shells through digital fabrication.

Paulo B. Lourenço is a full professor of Structural Engineering at the University of Minho, Portugal. He is a leader of the revision of the European Masonry code (Part 1-1). Paulo is experienced in NDT, advanced experimental and numerical techniques, innovative strengthening techniques, novel masonry products and earthquake engineering. He is a specialist in structural repair, conservation and strengthening, with works in more than 100 monuments.

1 Introduction

Throughout the world, masonry has been the most popular building material for centuries. It is a heterogeneous quasi-brittle material, which is a combination of units bonded together with mortar, often categorized as homogenous. Brick masonry comprising solid fired clay brick units and cement-lime-mortar are very popular in the UK as well as in many other countries. Its spread is most likely connected to the availability of the base materials at low cost and the ease of fabrication process that do not require high-skilled workers. Brick masonry's structural response depends on the mechanical properties of its components (unit and mortar) and the bond properties of the brick unit-mortar interface. Lourenco (1996) emphasized that brick masonry exhibits distinct directional properties due to the mortar joints, which act as planes of weakness. Masonry structures also show complex and non-linear mechanical behaviour. Meanwhile, the concept of simulating the mechanical behaviour of masonry structures using finite element analysis (FEA) has drawn much attention recently but the source of input material parameters such as strength and stiffness for the analysis remains a true challenge.

Angelillo (2014) explained that there are two approaches for getting materials properties for FEM of masonry structures. This is either by a simple assumption of material properties of general masonry or through detailed mechanical description of specific masonry materials. Both approaches have been used in the numerical analysis of masonry structures (Lourenco (1996), Lucchesi et al. (1996), Lourenco et al. (2007), Milani and Lourenco (2013) and Silhavy (2014)). However, it has been demonstrated that the first approach produces results that are affected by the assumptions made (Angelillo, et al., 2014). The latter approach can lead to more reliant results that are closer to reality. Indeed, Lourenco (1996) earlier works had suggested that a proper coordination and comparison between experimental work and numerical analysis can produce reliable and useful properties data for detailed numerical models.
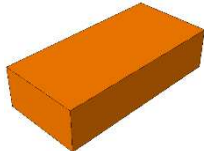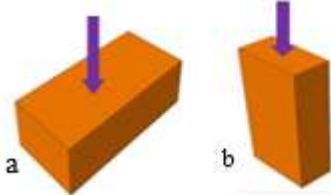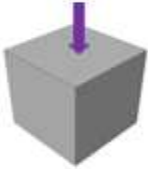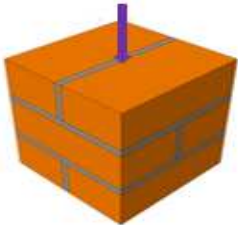
Therefore, this paper presents a numerical and experimental characterization of brick masonry components (solid fired clay brick and cement-lime mortar). The focus is to obtain accurate mechanical properties of the unit, mortar and the interfacial properties of the unit-mortar joint that is necessary to produce a detailed micro-modelling of masonry structures. To achieve this, a complete description of each component was done based on the experimental results of compression tests on bricks, mortar and the masonry assemblage (Dauda et al., 2018). For the post-peak behaviour of compressed brick and mortar, the concrete damage plasticity model in ABAQUS was used to characterise the nonlinearity of the units and mortar in both tensile and compression regimes. As required, a close coordination between the experimental work and numerical model was done by calibrating the model to develop a well fitted numerical model that represents the complex behaviour of units and mortar working together as masonry. The purpose of this study is to obtain strength material properties for unit, mortar and interface that will be used to analyse the out-of-plane response of masonry panels retrofitted with a new technique. As such, the authors have carefully obtained values experimentally and numerically using guidelines from existing literature. The obtained parameters were then calibrated and validated with the experimental data on a masonry cubic specimen.

Subsequent to this introduction section, the experimental characterization of mechanical properties of masonry components (UK fired clay solid bricks and mortar) and the compressive strength of a masonry cubic specimen is presented in section 2. In

section 3, the numerical analysis by finite element developed in ABAQUS to predict the behaviour of the masonry cubic specimen is presented based on the detailed micro-modelling techniques. The result of the numerical analysis is presented in section 4 and the conclusion is provided in section 5.

2   Experimental Program

Table 1: Experimental test matrix

Category		Properties	Relevant code
Brick Unit		Dry density	BS EN 772-13:2011
		Water absorption	BS EN 772-21:2011
	Load on (a) bedface (b) head	Compressive strength	
		Modulus of elasticity	BS EN 772-1:2011
		Poisson's ratio	
Mortar	Consistency of fresh mortar	Dropping value	BS 4551:2005
		Flow value	BS EN 1015-3:1999
		Compressive strength	BS EN 1015-11
Masonry Cube		Compressive strength	Conventional test with insight from BS EN 1052-1:1999

In order to characterize the mechanical behaviour of brick masonry, an experimental program has been developed based on the components and assemblage as follows: (i) brick unit characterization, (ii) mortar characterization and; (iii) masonry characterization. To characterize the brick unit (i), experimental tests were carried out to determine the water absorption, dry density, compressive strength, modulus of elasticity,

and Poisson's ratio of brick unit. The mortar behaviour (ii) was captured by analysing the consistency of fresh mortar and the compressive strength of hardened mortar. Each test was carried out according to the relevant European Norm (EN), as identified in table 1. Finally, an unconventional test was also carried out to determine the compressive strength of masonry composite (215 x 215 x 215mm masonry cubic specimen). In the following subsections each test is described in detail.

2.1   Characterization of brick unit

Six samples of engineering class B fired clay solid brick (UK standard size 215 x 102.5 x 65mm) were selected randomly from a brick package and tested in dry condition. The dry density (γ_{du}) of the bricks was determined according to (BS EN 772-13:2000) to indicate the general quality and conformity of the brick to manufacturer specification. The bricks were conditioned to constant mass by drying them in an oven at 100°C temperature for 48hrs, the dry weight and dimensions of the bricks were then obtained using weighing balance and measuring ruler respectively. The γ_{du} was calculated starting from the weight and volume of the bricks. Thereafter, the water absorption (w_u) was determined according to (BS EN 772-21:2011) to determine the durability of the bricks. For this reason, the bricks were immersed in cold water for 24hrs and the weight of the saturated bricks was obtained within 2mins after removal from the water. The increase in mass of the brick gives the water absorption of the bricks.

The compressive strength (f_b) of the six bricks was determined according to (BS EN 772-1:2011). Compressive strength of masonry depends on the compressive strength of the brick unit and is essential for design and retrofit of masonry. The specimens, after conditioned to a constant mass, were laid and centred on the platen of a 5000KN capacity compression-testing machine with 2mm thick plywood placed top and bottom face of the brick. A uniformly distributed load was applied gradually in equal increments of 4kN/sec up to failure. The loading and the results were monitored using a data logger connected to the machine and f_b was calculated from the failure load and loaded area of the brick. To estimate the strength of the bricks in two orientations, three bricks were loaded on header and bed face respectively, as shown in figure 1(a).

The modulus of elasticity (E_b) was determined using the stress-strain relationship obtained from the axial compression test. Before, placing the bricks under compression machine, FLA-5-11 strain gauges were fixed in longitudinal and along lateral direction on each brick (Fig. 1a) to record the strain values under axial compression. E_b was calculated by considering values between 30% and 60% of the maximum stress, according to Oliveira et al. (2012) and Vasconcelos and Lourenço (2009). Also, Poisson's ratio (μ_b) was calculated by plotting the lateral strains against longitudinal strains of each brick. Best line of fit was then plotted to determine the relation between the lateral and longitudinal strain. E_b and μ_b were only determined for bricks loaded in bed face because the masonry cubic specimens tested in section 2.3 were constructed with brick laid in bed face.

2.2   Characterization of mortar

Type N (general purpose) mortar mix with ratio of 1:1:6 (cement: lime: sand) was prepared. The amount of water to be added to mix proportion is not mentioned in standards, hence the water content that gives a working consistency was found by trial and error using the dropping ball test described in BS 4551:2005. The target dropping value of 10 +/- 0.5mm was achieved after three trials with a w/c ratio of 1.8. Thereafter,

the consistency of the fresh mortar was determined by flow test using BS EN 1015-3:1999.

Three samples of a 100 x 100 x 100mm cube were prepared and cured for 28days and tested under compression testing machine to determine the compressive strength of the mortar (f_m) (Fig. 1b). The specimens were carefully aligned under the machine with the centre of the ball-seated platen, so that a uniform seating is obtained, and a uniformly distributed load was applied gradually in equal increments continuously at 1kN/sec up to failure. f_m was calculated from the failure load and loaded area of mortar.

2.3   Characterization of masonry cubic specimen

The purpose of this test is to understand how bricks and mortar work together. It is an unconventional test developed according to previous tests carried out by Arash (2012). Six masonry cubic specimens (MC) of 215 x 215 x 215mm were prepared using masonry units from the same stock as the ones tested earlier and a 10mm thick mortar joint described above. The MC specimens were constructed using English bond consisting of alternate rows of headers and stretchers which is the oldest form of brick bond popular until the late 17th century (Anon, 2009). The MCs were prepared in the laboratory and horizontal level surface is ensured by using a bubble level during construction. After the construction, each sample was wrapped with polythene sheet for 14days and thereafter open and cured further for 14days in the laboratory to allow the samples to achieve its standard strength. An attempt to measure the deformation of the MC was made by attaching four LVDTs to the MC before testing (Fig. 1c). The specimens were carefully aligned with the centre of the ball-seated platen, under compression testing machine with 2mm thick plywood placed top and bottom under compression testing machine. A uniformly distributed load was applied gradually in equal increments continuously at 4kN/sec rate up to failure.

2.4   Experimental results and analysis

Table 2: Mechanical properties of brick units

Property	Values		Requirement
	Experiment	Manufacturer	
γ_{du} (kg/m^3)	2200	2310	shall not be less than 2079kg/m^3 i.e 90% of specified density (BS EN 772-13:2000)
W_u (%)	3.9	≤ 7	shall not be more than manufacturer limit (BS EN 772-21:2011)
f_b (N/mm^2)	87.9	75	shall be not less than the declared compressive strength (BS EN 772-1:2011)
E_b (N/mm^2)	32470	≤ 34000	between 3500 and 34000
μ_b [\]	0.26	0.3-0.5	range for clay masonry unit

The average value of the observed mechanical properties obtained from the experiments conducted on the brick units were presented in figure 2. The obtained brick properties were compared to the values declared by manufacturer except for E_b and μ_b

that were compared with values reported in Oliveira et al. (2012), Vasconcelos and Lourenço (2009) and Italian Code for Constructions (DM 14.1.2008) (Table 2). For the compressive strength, BR1, BR2 and BR3 were considered because the bricks were loaded in bed face. The strains plot for BR5 is too scatter and the line of fit does not seem best, hence the result was discarded and μ_b was calculated using results for BR4 and BR6. Generally, the results indicate that bricks are of good quality and conform to specification, making it acceptable for the proposed experiment.

For the fresh mortar, the mix ratio of 1:1:6 with w/c ratio of 1.8 gives the dropping value of 10.2mm and the corresponding mean flow value is 167mm. The consistency of mortar is good as this agrees with the ideal flow value (150-175mm) for mortar joints, as derived from Haach et al. (2007). The hardened mortars have an average strength (f_m) of 7.1N/mm^2 (Fig. 3).

Furthermore, the average compressive strength of the masonry cubic specimen obtained from experiments is 46.4N/mm^2. The 5% fractile value of compressive strength of the cubic specimen was found to be 41.4N/mm^2 according to the provision of section 10.2 of BS EN 1052-1:1999. Meanwhile, BS EN 1996-1-1:2005 described that compressive strength of masonry can be calculated using the properties of the units and mortar according to equation 1. The calculated value of 22.5N/mm^2 is 45% lower than what was gotten experimentally. This seems acceptable because the calculated value is characteristic and is a lower bound of many tests.

$$f_k = K \times f_b^{\alpha} \times f_m^{\beta} \qquad\qquad (1)$$

where;

f_k : is characteristic compressive strength of masonry;
f_b : is compressive strength of masonry unit, in the direction of the applied action
f_m: is compressive strength of the mortar
K: is a constant, function of the type of masonry units and mortar (0.55 in this case)
$\alpha\ and\ \beta$: are constants, for general purpose mortar =0.7 and =0.3

Clearly, the strength obtained for the bricks and mortar shows that the brick is a strong unit while the mortar is a weak joint, which makes the combination a strong unit-weak mortar joint connection, a typical characteristic of old masonry structures.

2.5   *Masonry specimen failure mode*

The observation of the images after the test shows that the failure modes are brittle. A view through the casement and video recorded during the tests indicate that the failure of the units (Fig. 4a) starts with a vertical crack along the height of the bricks causing a high tensile stress in the bricks which make them to fails ultimately.

The failure was characterized by vertical splitting cracks appearing firstly in the central unit and extending to other units as the stress increases. This observation is similar to what was reported by Vasconcelos and Lourenço (2009) and Mohamad and Chen (2016). This failure pattern is due to presence of the vertical joints and possibly also the lateral expansion of the mortar inducing high tensile strength in the bricks. As can be seen from figure 4b, the MC split on the faces caused the attached LVDTS on the surface to fall off which make recording the deformation difficult because the compression machine does not have an inbuilt LVDT.

3   Numerical Analysis

Computational numerical analyses are basic skills employed by engineers as a useful complement or alternative to experimental tests. They are capable of predicting the behaviour of structures to applied load. Numerical analyses are based on different theories such as finite element model (FEM), discrete/distinct element methods (DEM) or particle flow code (PFC), among others (Lourenco (1996), Asteris et al. (2015), and Zhang et al. (2016)). FEM-based models are the most widely used due to the availability of a large number of analysis software that operates based on this theory. Therefore, the numerical modelling strategy employed in this study is based on FEM.

Anthoine (1992), CUR (1994), Lourenco (1996), and Maccarini et al. (2018) among many other researchers who have previously worked on FE modelling of masonry structures agree that numerical modelling and analysis of masonry structures posed some of the greatest challenges to structural engineers. The main difficulty has been attributed to the presence of mortar joints, which act as planes of weakness, discontinuity and nonlinearity. Most importantly the existence of uncertainties in the material and geometrical properties is also another concern when modelling masonry structures (Lourenco (1996), Asteris et al. (2015), and Dogariu (2015)). In spite of these challenges, three modelling techniques (Fig. 5) have evolved.

[1] Detailed micro-modelling: Masonry is modelled as a three-phase material. The masonry units and mortar in the joints are represented by continuum elements while the unit–mortar interface is represented by discontinuous elements (Fig. 5a).

[2] Simplified micro-modelling: In this strategy, the bricks are represented as fictitious expanded bricks by continuum elements. The mortar joint is modelled as an interface with zero thickness (Fig. 5b).

[3] Macro-modelling: Masonry is modelled as one phase material by smearing out masonry units, mortar and unit–mortar interface in a homogeneous continuum (Fig. 5c).

The choice of the method to adopt depends on the level of information available, accuracy and simplicity desired (Lourenco, 1996). The detailed micro-modelling technique produces the most accurate results, although it is computationally intensive due to the detailed level of refinement. Therefore, this study adopts the detailed micro-modelling technique to perform a numeric simulation of the masonry specimen. The calibration and validation of the FE model were done using the experimental results and observed failure modes.

3.1   Description of FE model

The masonry cubic model was created using three-dimensional solid (or continuum) elements in ABAQUS. In particular, hexahedral 8-node linear brick, reduced integration, hourglass control (C3D8R) which has an improved convergence and accuracy was selected to generate the mesh that represents the brick unit and mortar joint. The size of the unit is 215 x 102.5 x 65mm and the thickness of mortar joint is 10mm. The brick unit and mortar joint (bed and perpendicular) were defined using their respective own mechanical properties. The nonlinear behaviour of brick unit and mortar

both in compression and tension regime have been accounted for in the FEs model using the constitutive model (concrete damage plasticity (CDP)). The brick-mortar bond failure behaviours have also been considered using the nonlinear cohesive interfaces. In addition, the contact penalty approach was enforced for the interaction between the brick and mortar interface. For the boundary condition, the nodes at the top of the cubes were restrained in x and z direction while the bottom nodes were restrained in all three directions (x, y, and z) to replicate the friction in test condition of the specimen. The Static General step in ABAQUS standard/explicit was selected for the analysis. Figure 6 shows the general assemblage of the masonry specimen, FE mesh and the boundary condition.

3.2 *Properties of brick unit and mortar*

Obtaining exhaustive experimental data appropriate for detailed micro-modelling of masonry structures has sometimes proved tedious. Compression tests are the easiest and most reliable test on materials, particularly when the post-peak regime is captured. Compression tests allow to fully characterize the material behaviour in form of a stress-strain curve, which is a requirement to accurately perform nonlinear finite element.

The concrete damage plasticity (CDP) constitutive model available in ABAQUS and Guo (2014) was used to simulate the tensile and compressive non-linear behaviour of unit and mortar. The CDP model assumes a non-associated potential plastic flow, which is an adoption of Drucker-Prager hyperbolic function for flow potential. The failure modes recognised by CDP models are cracking in tension and crushing in compression.

For the brick unit, the tensile and compressive plastic-damage nonlinear properties were calculated from the typical stress-strain response of brittle material under uniaxial loading. Figure 7 shows the behaviour in compression regime. The curve has three different regions derived from Sinha et al. (1964), Guo (2014), and Santos et.al (2017). The compressive strength $(f_{c,b})$ and modulus of elasticity (E) of the brick units obtained experimentally were used in these equations. Haven obtained $f_{c,b}$, the stress-strain relationship in compression regime are assumed to be consistent with the compressive fracture energy $(G_{f,c})$, which is equal to the area under the curve in figure 7a. For the present study, an average ductility index in compression $(d_{u,c} = 0.33mm)$ which is the ratio between the compressive fracture energy and the compressive strength is used to obtain the approximate fracture energy (Angelillo et al., 2014). So, once the compressive strength of the brick unit $(f_{c,b})$ and the peak strain obtained directly from the experiment has been fixed, then the brittleness parameter is chosen to ensure that the area under the curve is equalled to $(G_{f,c})$. Correspondingly, figure 8 shows the behaviour of the brick unit in tensile region. The ductility index in tension $(d_{u,t} = 0.018mm)$ which is a ratio between the fracture energy $(G_{f,t})$ and the tensile strength $(f_{t,b})$ was used to obtain the fracture energy (Pluijm (1992), Lourenco (1996, 2002) and Angelillo et al. (2014)).

Similarly, for mortar an average ductility index in compression $(d_{u,c} = 1.6mm)$ is used to obtain the approximate compression fracture energy. Consistently, using the available information provided by Pluijm (1992), Lourenco (1996, 2002) and Angelillo et al. (2014), the ductility index in tension $(d_{u,t} = 0.065mm)$ was used to obtain the tensile fracture energy. In order to plot the strain-strain relationship to simulate the behaviour of

the mortar, the procedures highlighted in BS EN 1992-1-2:2004, Wang and Hsu (2001) and Guo (2014) were followed. The only available direct measurement from the tests is the mortar compressive strength ($f_{c,m}$). Other quantities such as longitudinal modulus of elasticity ($E_{c,m}$) of the mortar and shortening strain were calculated using the equations. 2-6.

Referring to figure 9 for damage plasticity of mortar under uniaxial compression, the compressive stress was calculated as follows and the plot of data obtained was compared to the standard chart given in BS EN 1992-1-2:2004.

$$\sigma_c = f_{c,m}(k\eta - \eta^2)/(1 + (k - 2)\eta) \tag{2}$$
$$k = 1.05 E_{c,m} * (\varepsilon_{c1}/f_{c,m}) \tag{3}$$
$$\eta = \varepsilon_c/\varepsilon_{c1} \tag{4}$$
$$E_{c,m} = 22 * (f_{c,m}/10)^{0.3} \text{ in GPa} \tag{5}$$
$$\varepsilon_{c1} = 0.7 * (f_{c,m})^{0.31} \tag{6}$$

Referring to figure 10 for damage plasticity of mortar under uniaxial tension, the tensile strength of the mortar was not determined experimentally but equation 7 stated in (BS EN 1992-1-2:2004) was used to calculate this. To simulate the tensile behaviour of mortar, equations 8 and 9 were used. The tensile stress of mortar can be linearly reduced to zero, starting from the moment of reaching the tensile strength, this was done and the resulting stress-strain curve was compared to the description in ABAQUS and BS EN 1992-1-2:2004) as shown in figure 9.

$$f_{t,m} = 0.3 * (f_{c,m})^{2/3} \tag{7}$$
$$\sigma_t = E_{c,m} * \varepsilon_t \quad if \ \varepsilon_t \leq \ \varepsilon_{cr} \tag{8}$$
$$\sigma_t = f_{c,m} * (\varepsilon_{cr}/\varepsilon_t)^{0.4} if \ \varepsilon_t > \ \varepsilon_{cr} \tag{9}$$

3.3   General parameter for CDP of brick and mortar

Apart from the above-presented damage plasticity data, other parameters are needed for application of CDP for quasi-brittle materials in ABAQUS. These parameters are defined as follows:

- Dilation angle (Ψ): this parameter is essential because it controls the amount of plastic volumetric strain developed during plastic shearing and is assumed constant during plastic yielding. The value of $\psi = 30^o$ corresponds to clay's angle of internal friction was adopted in this study (Lubliner, et. a1, 1989)

- Eccentricity parameter (*e*): this value ranges from 0-0.1 from theory of Drucker-Prager. A value of e = 0 means the yield surface in the meridian planes is straight line while e = 0.1 means the yield surface takes a shape in form of a hyperbola. For this study, an intermediate eccentricity (e = 0.05) was assumed.

- Bi and unidirectional compressive strength ratio (f_{bo}/f_{co}): this is the ratio between the bidirectional compressive strength of masonry and unidirectional compressive strength of masonry. In this study, the default value equal to 1.16 was used in ABAQUS.

- Stress ratio in tensile meridian *(k)*: this is the ratio of the second stress invariant on the tensile meridian and it basically implemented for viscoplastic regularisation of constitutive equation in ABAQUS. This study used 0.67 default value in ABAQUS.

- Viscosity parameter: the main function of this parameter is to facilitate the numerical analysis convergence process in ABAQUS without affecting the result. Based on a preliminary study, a low value of 10^{-5} is chosen in this study.

3.4   Properties of brick-mortar interface

In the present case, the response of the assemblage is controlled mostly by the mortar tensile strength and fracture energy, which mainly depends on the interaction of the unit-mortar interface. In this model, the interaction between the brick units and mortar is defined in the interaction module of ABAQUS. Surface-to-surface contact was implemented in the model using the three contact behaviours, which are explained below:
- Normal behaviour: hard contact behaviour normal to the surfaces is selected. The purpose is to prevent interpenetration of surfaces, and also to allow a separation between them once a contact has been established.

- Tangential behaviour: When surfaces are in contact, they usually transmit shear and normal forces across their interface (Fig. 11). Thus, the analysis needs to take frictional forces, which resist the relative sliding of the surfaces, into account. Here, Coulomb friction was used to describe the interaction of contacting surfaces. This model characterizes the frictional behaviour between the surfaces using a coefficient of friction (μ). The penalty friction formulation used is μ = 0.75.

- Cohesive behaviour: Mohamad and Chen (2016) examined different researches conducted on defining the cohesive interaction performance for quasi-brittle materials. Mohamad and Chen (2016) recognized that the traction-separation method is the most adopted and it is highly compatible with ABAQUS. Zheng et al. (2016) state that traction separation law involves three criteria: linear elastic behaviour (Eqn. 10), a damage initiation criterion and a damage evolution law.

$$\begin{bmatrix} t_n \\ t_s \\ t_t \end{bmatrix} = \begin{bmatrix} K_{nn} & & \\ & K_{ss} & \\ & & K_{tt} \end{bmatrix} \begin{bmatrix} \varepsilon_n \\ \varepsilon_s \\ \varepsilon_t \end{bmatrix} \tag{10}$$

To estimate this linear elastic behaviour, which is stiffness interface expressed in the matrix in equation 22, a high penalty stiffness was adopted (D'Altri et al., 2018) to remove any penetration between elements. The default penalty stiffness was used. This contact leads to stiffness degradation, in which it is only necessary to specify the interface mode I fracture energy ($G_f{}^I$). The value specified in this model ($f_t = 0.36\,N/mm^2$ and $G_f{}^I = 0.012\,N/mm$) was derived from the tensile behaviour of the interface (purple line) in figure 12,

which shows a good agreement with experimental results obtained in Pluijm, 1992 (Lourenco, 1996).

3.5   Calibration of the numerical model

The numerical model was calibrated in the following four steps: (i) first, reference material elastic properties were estimated based on the results of the compression tests; (ii) the Poisson's ratio properties and coefficient of friction were further adjusted based on the comparison of the numerical results with those obtained in the experiments; (iii) the CDP nonlinear material properties were adjusted based on the comparison of the stress-displacement envelope obtained with the one given in ABAQUS using the ductility index and fracture energy data founds in Pluijm (1992), Lourenco (1996), Angelillo (2014), and Silva et.al (2018); (iv) lastly, the influence of the mesh density i.e approximate global size of mesh was investigated (Fig. 13). The loading and boundary conditions were kept the same throughout the mesh global seeds size variation.

4   Results and discussion

Table 6 shows the result from the mesh sensitivity study. The analysis revealed that using a coarse mesh size (MS) of >= 15 causes difficulty in obtaining convergence. The results were not acceptable, due to a large error and no convergence upon coarse mesh refinement. The results obtained from fine mesh sizes (2.5, 5, 7.5 and 10 mm) converge well. The maximum stress obtained does not change significantly with a coefficient of variation (cov) of 1.6% and are in agreement with the experimental results. Since ABAQUS only allocates memory as needed during analysis, an increase in memory allocation was needed for computations when using smaller mesh sizes. For instances, when the mesh size was reduced from 10 to 5 mm, the memory allocation was increased from 9.7GB to 15.9GB (64% increment). This implies that too dense mesh requires a large amount of computer memory and long run times especially for a nonlinear analysis of this type. Therefore, the most suitable mesh size considering balance between accuracy, time and resources is MS10. The computational time with this mesh size is approximately 211secs with 98% accuracy to that of 5mm size mesh, which requires 738secs when using a computer equipped with a processor intel ® core ™ i5-6400 CPU@ 2.70 GHz and 16 GB RAM.

Table 4: Mesh convergence results

Mesh size (mm)	Numerical	Experimental	Time (secs)	%Error
2.5	49.47	46.40	3435.00	6.61
5.0	48.91	46.40	1834.00	4.98
7.5	48.26	46.40	1043.00	4.01
10.0	47.75	46.40	211.00	2.91
15.0	42.81	46.40	143.00	-7.74

The influence of the mesh density was further investigated by comparing the stress vs strain plot for each mesh size as shown in figure 14. Except for the case of MS15, decreasing the mesh size further produces only minor increases in peak stress and strain. For all the mesh sizes, the stress-strain curve has a good match up to 28 N/mm^2 (60% of the maximum stress obtained experimentally). This is the region where the model is in linear behaviour. However, for the non-linear region, the mesh sizes still produce comparable curves that predict the experimental value with the exception of MS15, for which a strength equal to 42.8 N/mm^2 is obtained , which is lower than what was obtained in the experiment. Therefore, a mesh size lower than 15 is recommended. As such, MS10 was used in this study in order to save resources while still maintain the accuracy of the model.

Figures 15 show the stresses contour and the damage contour plots obtained numerically for the masonry cubic specimen. The principal stress is compared to the average compressive strength of the specimens obtained experimentally. The maximum stress obtained from the numerical model is 48.7 N/mm^2. This value is only 5% different from the average compressive strength of masonry obtained from the experiment (46.4 N/mm^2).

Significantly, the failure mode observed in the model output (Fig.15) is similar to what was observed experimentally with the maximum compressive stress occurring at the bottom edges of the cubic model. The stress diagrams also show that there is compressive stress in the bed joint and tensile stress in the perpendicular mortar joint. This tensile stress in perpendicular joint leads to lateral expansion of mortar joint, which then induce high tensile stresses in the brick units. Figure 15c shows a cut along y-plane of the cubic model to reveal the tensile stress distribution in the model. This figure shows areas of the cubic specimen where cracks are most likely to develop. The maximum principal stresses are an indication where cracks are likely to appear and the areas showing highest values (colours tending towards red at edges of the model) can be associated to the development of cracks. In figure 15c, the areas with coral and red colour represent the region that split off during the experiment upon full crack formation as the load increases. The splitting off of these parts then leads to an *hourglass shape* specimen after the failure (Fig. 15d). Figure 15d can then be liken to the inner region of the obtained stress diagram shown in figure 15c. Despite the modelling limitation that prevents the part that split off during the test to break off from the model output, the portions of higher concentration of the stress are well consistent with the portion that split off in the experiment (Fig. 15c vs Fig.15d).

Moreover, to validate the agreement in the experimental failure with the numerical failure pattern, the damage pattern obtained by the developed numerical model is represented in term of compressive damage (DAMAGEC) and tensile damage (DAMAGET) contour plot (Fig. 15e & 15f). By comparing the numerical damage with the observed failure pattern, tensile damage and thus cracking of the brick unit is clearly visible in the central part of the cubic model (Fig. 15f). In particular, the tensile stress in the perpendicular mortar joint in the middle course identified in the experiment is clearly represented in the numerical output. Also, compressive damage plot (Fig. 15e) shows that the bed joints failed in compression. These observations are in good agreement with the ones observed in the experimental failure patterns.

In order to describe the full behaviour of the model under continuous increase of load, stress-strain plot from static riks step (arc-length control) is shown in figure 16. The figure shows that the deformation (strain) increases as the stress increases until the peak stress is reached. After the peak stress is reached, softening i.e a gradual decrease of strength under a continuous increase in deformation is experienced. This is an ideal stress-strain diagrams for a quasi-brittle material such as masonry cubic specimen under uniaxial compression. The stress-strain performances (Fig. 16) show a first linear branch up to a stress of about 33 N/mm^2 and strain of 0,006. The stress at this point compares with (31 N/mm^2), the average stress obtained experimentally when the bricks start to split off) shows only 6% variation. To this effect, the stress-strain curve (Fig.16) can be divided into two stages viz linear elastic branch (uncracked stage) and parabolic inelastic branch (crack formation stage). To each crack formation was associated an increased strain till the reach of the peak load that causes the cubic specimen to fail by splitting. The peak stress and strain obtained numerically are 49 N/mm^2 and 0.0018 respectively.

5   Conclusions

This paper presents a numerical study and experimental tests to characterize masonry components (engineering class B fire clay solid brick units and mortar). The masonry unit and mortar characterised in this paper are currently being used to develop a new retrofit technique. An experimental work on brick units, mortar and an unconventional test on masonry cubic specimen has been carried out to study the behaviour of the specimens under compression loading.

Thereafter, a detailed micro model of the masonry cubic specimen was developed and analysed in ABAQUS. Based on the results of the compression tests on the brick units and mortar, nonlinear behaviour of masonry unit and mortar both in compression and tension regime have been estimated and accounted for in the developed FEs model using the constitutive damage plasticity model. Properties of the interfacial behaviour of the brick unit-mortar interface were also included in the model. The calibration and validation of the FE model were done using the experimental results and observed failure modes.

The following conclusions were drawn:

• The proposed masonry units and mortar mix ratio are suitable for the proposed experimental study because the combination of the two is similar to what is expected in old masonry units (strong unit-weak mortar joint). Hence, the material source remains unchanged throughout the ongoing experimental work.

• The developed FEs model of masonry cube was able to predict the behaviour and failure of masonry cube. The result gives a difference of 5% between numerical value and experimental value. This indicates that the model is able to predict the compressive strength of the masonry cubic specimen. However, the behaviour in the post peak regime has not been validated since more experimental data would be needed to substantiate this. Therefore, a more complete experimental analysis of the materials in the post peak regime is recommended.

References

Angelillo, M. (Eds.), (2014) Mechanics of Masonry Structures, CISM International Centre for Mechanical Sciences, Udine.

Angelillo, M., Lourenco, P. and Milani, G. (2014) 'Masonry behaviour and modelling', in Angelillo, M. (Eds.), *Mechanics of Masonry Structures*, CISM International Centre for Mechanical Sciences, Udine, pp.1-23.

Anon, B. (2009) 'Brick bonds: heritage directory notes'. *The Heritage Directory,* [Online] http://www.theheritagedirectory.co.uk (Accessed 22 Jan. 2017).

Anthoine, A. (1992) *In-plane behaviour of masonry: a literature review*, Report EUR 13840 EN, Commission of the European Communities, JRC - Institute for Safety Technology, Ispra, Italy.

Arash, S. (2012) 'Mechanical properties of masonry samples for theoretical modelling' in 15th International Brick and Block Masonry Conference, International Brick and Block Masonry, Florianópolis, Brazil.

Asteris, P., Sarhosis, V., Mohebkhah, A., Plevris, V., Papaloizou, L., Komodromos, P. and Lemos, J. (2015) *Numerical Modelling of Historic Masonry Structures*. Handbook of Research on Seismic Assessment and Rehabilitation of Historic Structures, pp.213-256.

British Standard Institution (1999) BS EN 1015-3:1999: *Methods of test for mortar for masonry - Determination of consistence of fresh mortar (by flow table)*. London, BSI.

British Standard Institution (1999) BS EN 1052-1:1999: *Methods of test for masonry-part1- Determination of compressive strength*. London, BSI.

British Standard Institution (2000) BS EN 772-13:2000: *Methods of test for masonry units - Determination of net and gross dry density of masonry units (except for natural stone)*. London, BSI.

British Standard Institution (2004) BS EN 1992-1-2:2004: *Eurocode 2 - Design of Concrete Structures - General rules structural fire design*. London, BSI.

British Standard Institution (2005) BS 4551:2005: *Methods of test for mortar and screed-chemical analysis and physical testing*. London, BSI.

British Standard Institution (2005) BS EN 1996-1-1:2005: *Eurocode 6 - Design of masonry structures - Part 1-1: General rules for reinforced and unreinforced masonry structures*. London, BSI.

British Standard Institution (2011) BS EN 772-1:2011: *Methods of test for masonry units - Determination of compressive strength*. London, BSI.

British Standard Institution (2011) BS EN 772-21:2011: *Methods of test for masonry units - Determination of water absorption of clay and calcium silicate masonry units by cold water absorption*. London, BSI.

CUR (1994) *Structural masonry: an experimental/numerical basis for practical design rules (in Dutch)*. Report 171, CUR, Gouda, Netherlands.

D'Altri, A., de Miranda, S., Castellazzi, G. and Sarhosis, V. (2018) 'A 3D detailed micro-model for the in-plane and out-of-plane numerical analysis of masonry panels' *Computers & Structures*, 206, pp.18-30.

Dauda, J., Iuorio, O. and Lourenco, P. (2018) 'Characterization of brick masonry: study towards retrofitting URM walls with timber-panels' *in IMC 2018: Proceedings of 10th International Masonry Conference. Milan, International Masonry Society*, pp.1963 - 1978.

Dogariu A. (2015) *Numerical analysis of a steel wire mesh seismic retrofitting techniques for masonry structures*. [online] http://www.bipcons.ce.tuiasi.ro/Archive/519.pdf (Accessed 18 May 2017).

Guo, Z. (2014) *Principles of Reinforced Concrete*, 1st ed., Oxford, pp.547-589.

Haach, V., Vasconcelos, G., Lourenço, P. and Mohamad, G. (2007) 'Composition study of a mortar appropriate for masonry cavities and joints' in *Proceedings of North American Masonry conference, The Masonry Society*, USA, pp.530-541.

Lourenco, P. (1996) *Computational Strategies for Masonry Structures*. PhD thesis, Delft University of Technology., Delft, Netherlands.

Lourenco, P. (1998) 'Experimental and numerical issues in the modelling of the mechanical behaviour of masonry', *Structural analysis of Historical Constructions, II*.

Lourenco, P., Milani, G., Tralli, A. and Zucchini, A. (2007) 'Analysis of masonry structures: review of and recent trends in homogenization techniques', *Canadian Journal of Civil Engineering*, 34(11): 1443-1457.

Lubliner, J., Oliver, J., Oller, S. and Onate, E. (1989) 'Plastic-damage model for concrete', *International Journal of Rock Mechanics and Mining Sciences & Geomechanics*, Vol 26 No. 5, pp.252.

Lucchesi M, Padovani, C. and Zani, N. (1996) 'Masonry like materials with bounded compressive strength*'*, International. *Journal of Solids and Structures*, Vol 33, pp.1961-1994.

Maccarini, H., Vasconcelos, G., Rodrigues, H., Ortega, J., and Lourenço, P., (2018) 'Out-of-plane behavior of stone masonry walls: Experimental and numerical analysis', *Construction and Building Materials*, 179, pp.430-452.

Milani, G. and Lourenco, P. (2013) 'Simple homogenized model for the non-linear analysis of FRP strengthened masonry structure*s* -. Part I: Theory'. *Journal of Engineering Mechanics ASCE*, 139(1), pp. 59-76. DOI: 10.1061/ (ASCE) EM.1943-7889.0000457.

Mohamad, A. and Chen, Z. (2016) 'Experimental and numerical analysis of the compressive and shear behavior for a new type of self-insulating concrete masonry system', *Applied Sciences,* 6(9), pp.245.

Oliveira, D., Silva, R., Garbin, E. and Lourenço, P. (2012) 'Strengthening of three-leaf stone masonry walls: an experimental research', *Materials and Structures*, 45(8), pp.1259-1276.

Pluijm R. (1992) 'Material properties of masonry and its components under tension and shear', in. In: *6th Canadian Masonry Symposium,* 15-17 June, 1992. Saskatoon, Canada.

Santos, C., Alvarenga, R., Ribeiro, J., Castro, L., Silva, R., Santos, A. and Nalon, G. (2017) 'Numerical and experimental evaluation of masonry prisms by finite element method'*, IBRACON Structures and Material Journal*, 10(2), pp.477-508.

Silhavy M. (2014) '. Mathematics of the masonry-like model and limit analysis', in *Angelillo*, M. (Eds.), *Mechanics of Masonry Structures*, CISM International Centre for Mechanical Sciences, Udine, pp.1-23.

Silva L., Lourenço P. and Milani G. (2018) 'Derivation of the out-of-plane behaviour of masonry through homogenization strategies: Micro-scale level', *Computer and Structures*, 209, pp.30-43.

Sinha, B., Gerstle, K. and Tulin, L. (1964) '. Stress-strain relations for concrete under cyclic loading'. *ACI Journal Proceedings*, 61(2), pp.195-211.

Vasconcelos, G. and Lourenço, P. (2009) '. Experimental characterization of stone masonry in shear and compression', *Construction and Building Materials*, 23(11), pp.3337-3345.

Wang, T. and Hsu, T. (2001) '. Nonlinear finite element analysis of concrete structures using new constitutive models', *Computers and & Structures*, 79(32), pp.2781-2791.

Zhang, S., Yang, D., Sheng, Y., Garrity, S. and Xu, L. (2016) '. Nnumerical modelling of frp-reinforced masonry walls under in-plane seismic loading', *Construction and Building Materials*, 134, pp.649-663.

Figures

Figure 1: Characterization of (a) masonry unit (b) mortar and (c) masonry cubic specimen
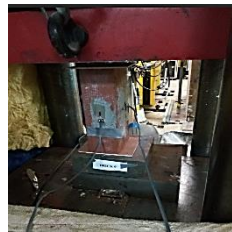
Load applied on head

Load applied on bedface

a)

Strain gauges on brick

Longitudinal Strain gauge   Lateral Strain gauge
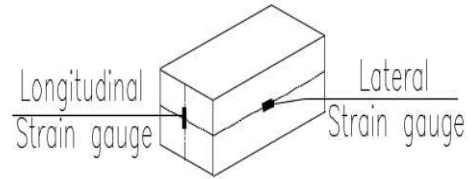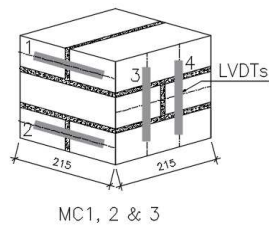

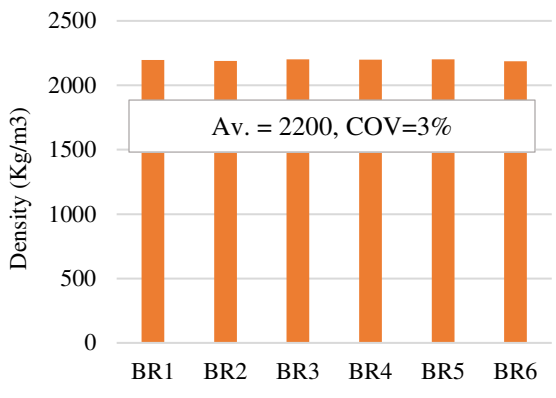
Flow table test for fresh mortar
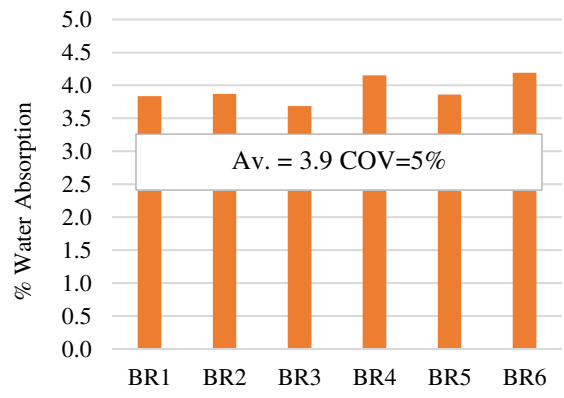
b)

Compression test on hardened mortar cube
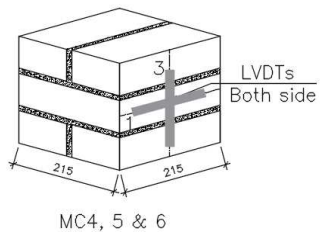
c)

Compression test on masonry cubic specimen

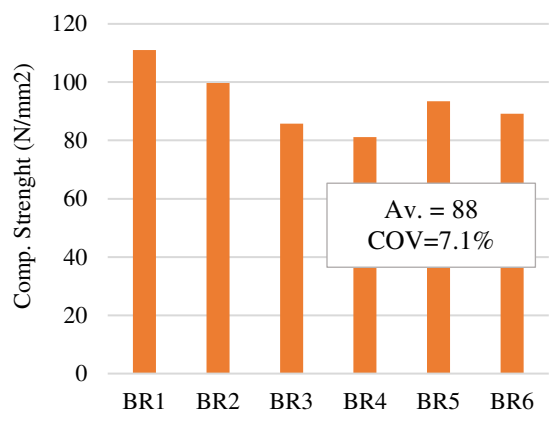Figure 2: Mechanical properties of brick unit; (a) density (b) water absorption (c) compressive strength (d) modulus of elasticity and (e) Poisson's ratio

a) Density of brick

b) % water absorption rate of brick

c) Compressive strength of brick
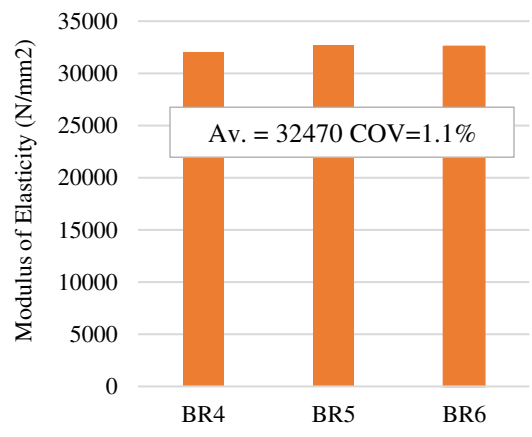
d) Modulus of elasticity of brick
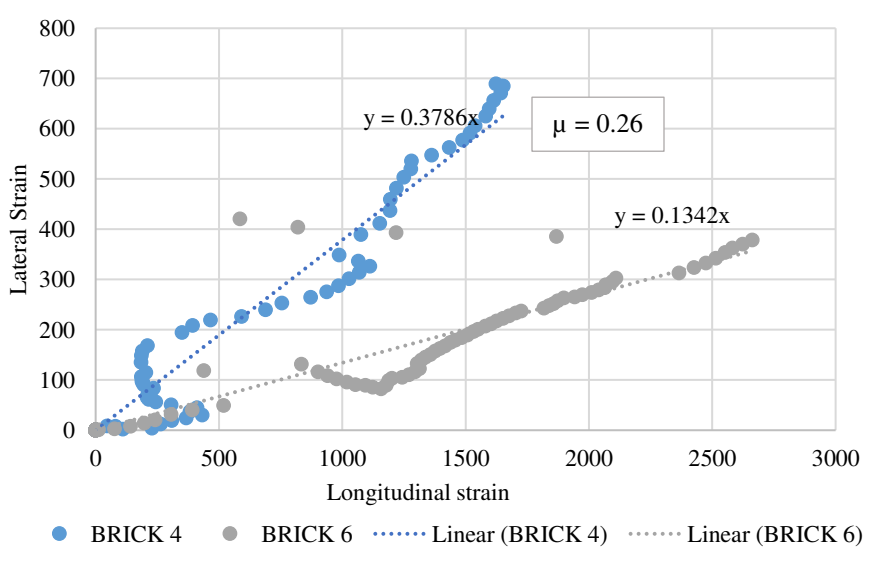
e) Poisson's ratio of brick

Figure 3: Mechanical properties of mortar; (a) consistency flow value (b) compressive strength of hardened mortar

a)

b)
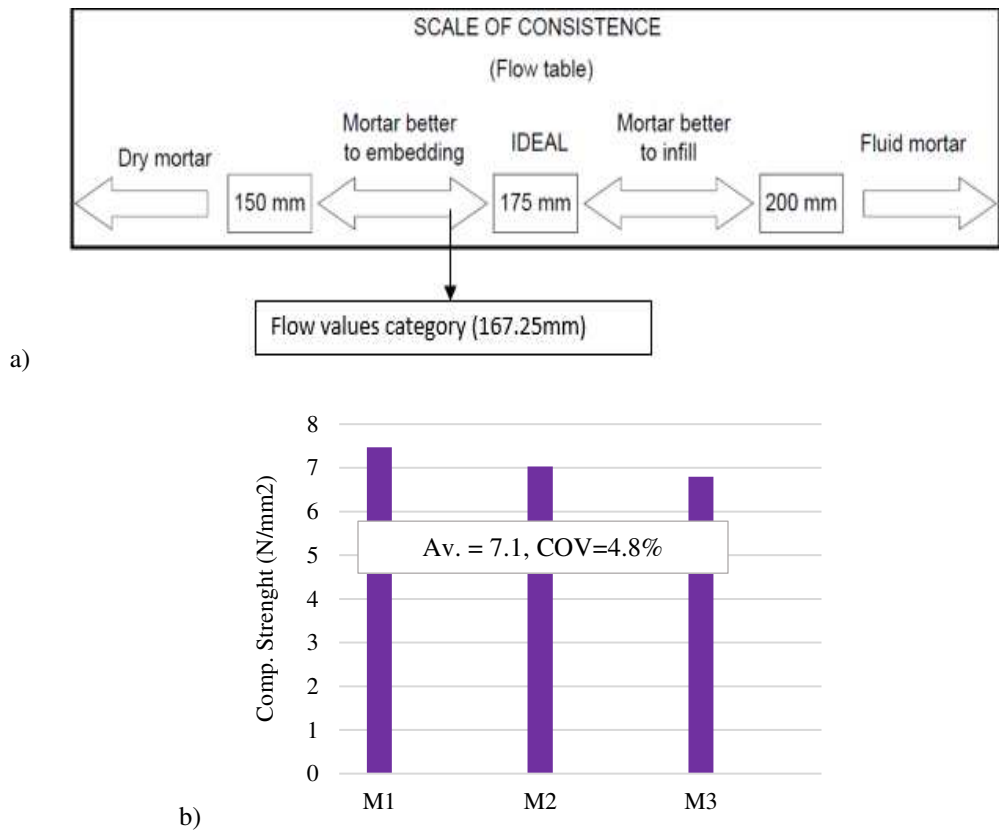
Figure 4: Failure modes of (a) brick units (b) masonry cubic specimen

BR1

BR2

BR3

BR4

BR5

BR6

a)

MC1   MC2   MC3

b)

MC4   MC5   MC6
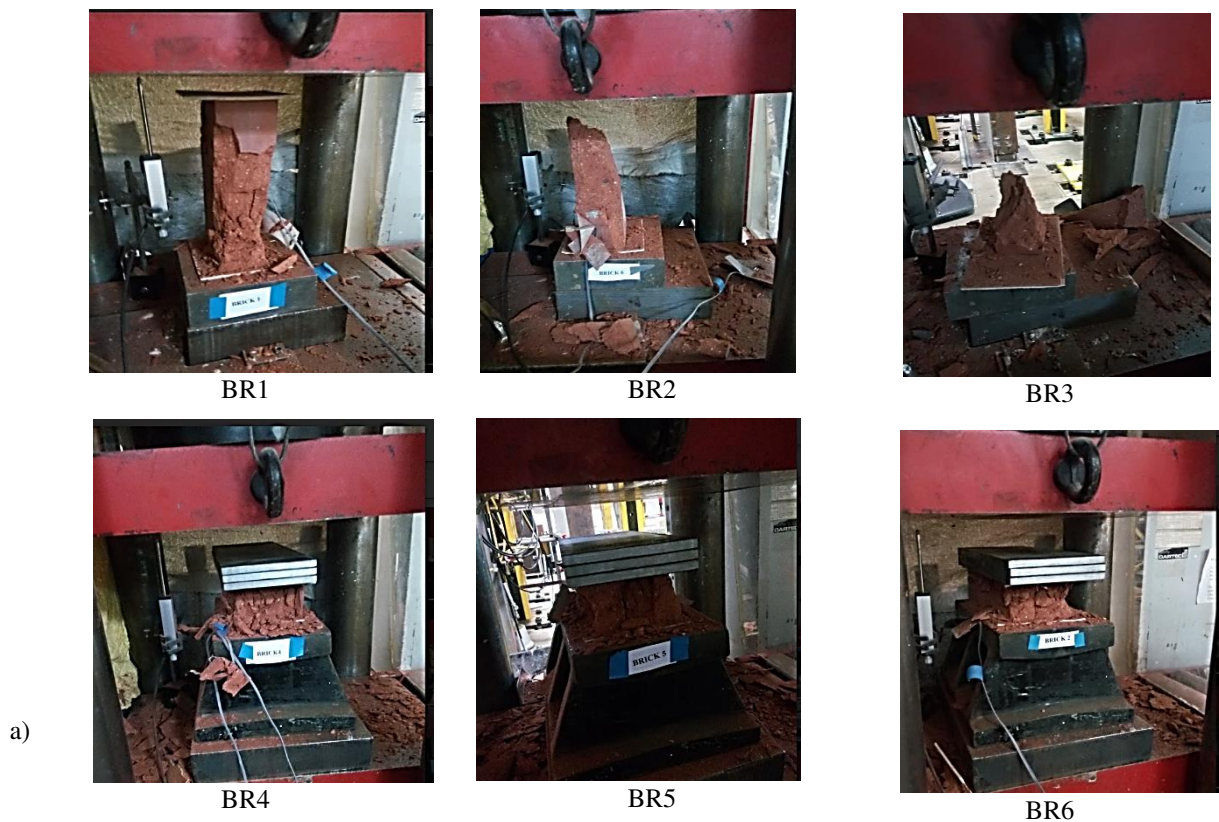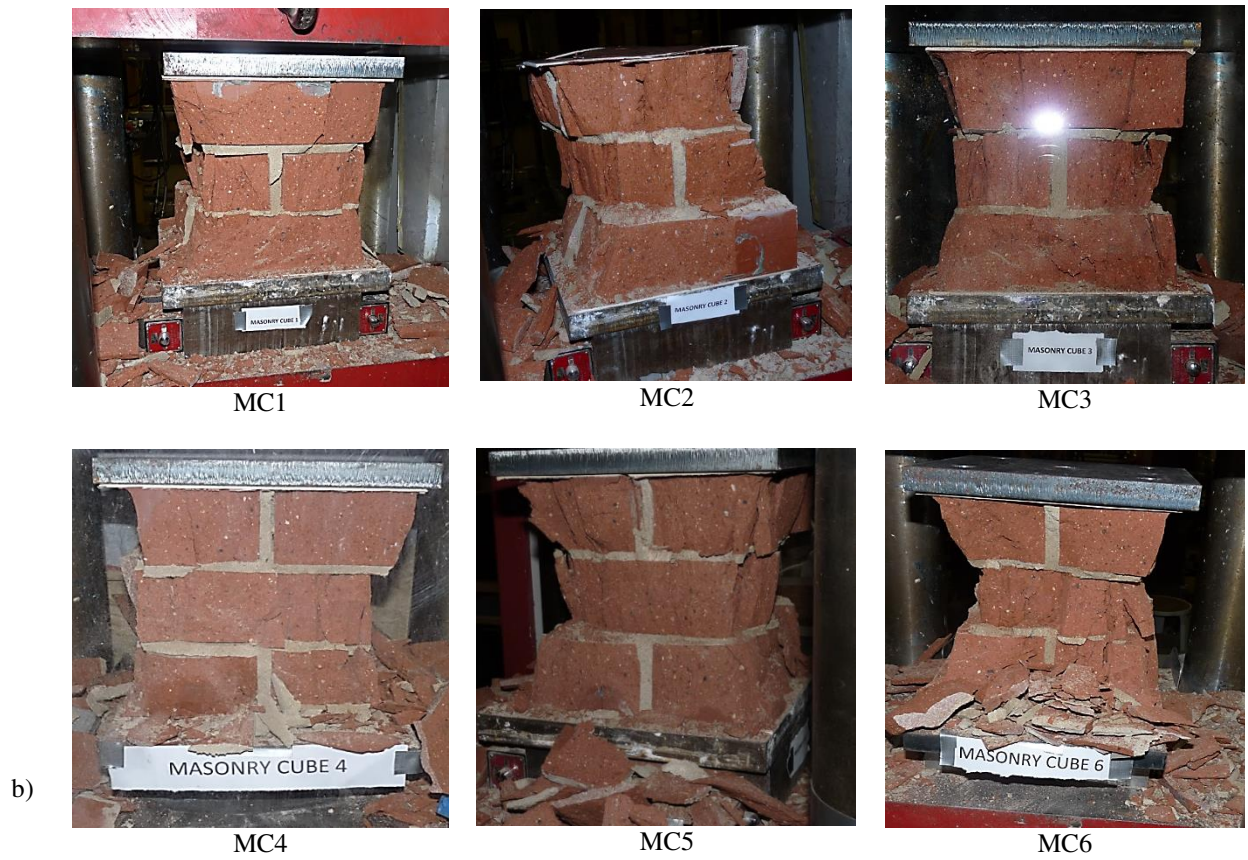
Figure 5: Masonry modelling techniques (a) real masonry sample (b) detailed micro-modelling (c) simplified micro model and (d) macro modelling

Mortar
Brick

a)   Real masonry sample

Mortar continuum
nonlinear model

Brick continuum
nonlinear model

Brick-mortar
nonlinear interface

b)   Detailed micro-model

Block continuum
linear/nonlinear
model

Joint nonlinear
interface

c)   Simplified micro-model

Homogenized
continuum
nonlinear model

(No interfaces)
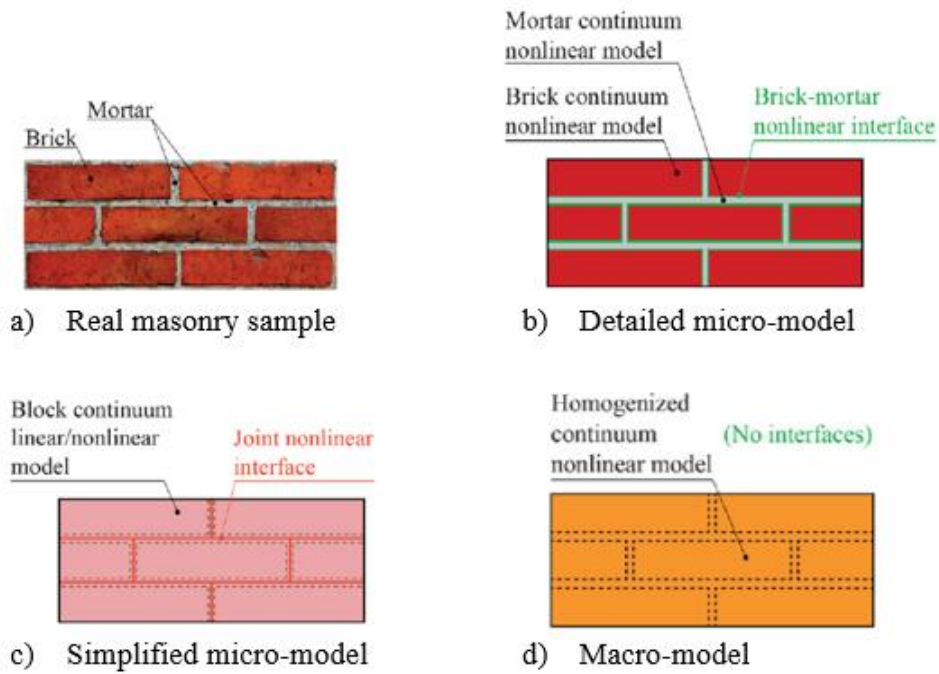
d)   Macro-model

Figure 6: a) Micro modelling of masonry cubic specimen, with (b) front elevation, (c) mortar joint, (d) side elevation, and (e) FE mesh, boundary condition and surface interaction
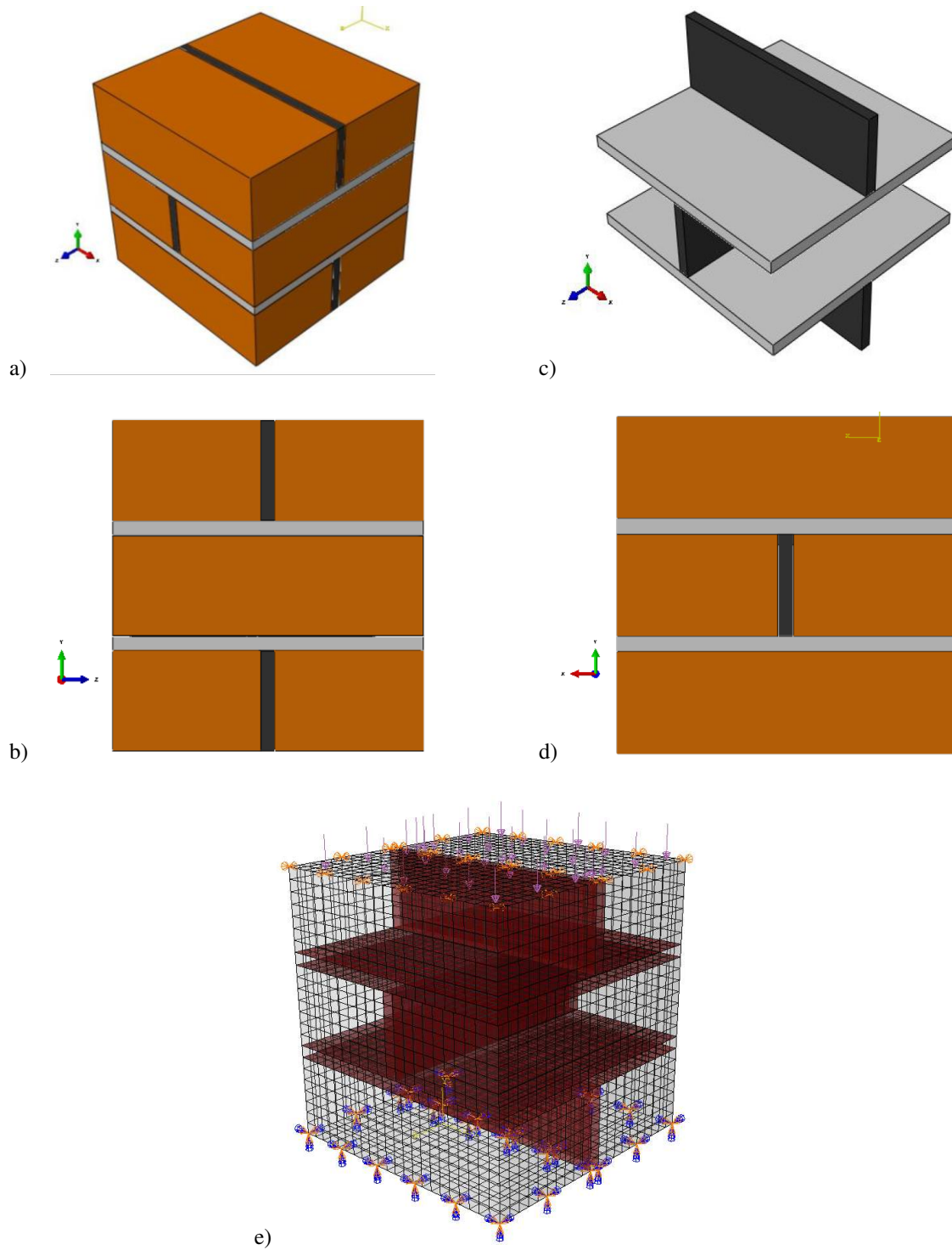
Figure 7: Masonry unit behaviour under uniaxial compression (a) numerical model (b) typical response in ABAQUS (Simulia, 2014).

a)

b)
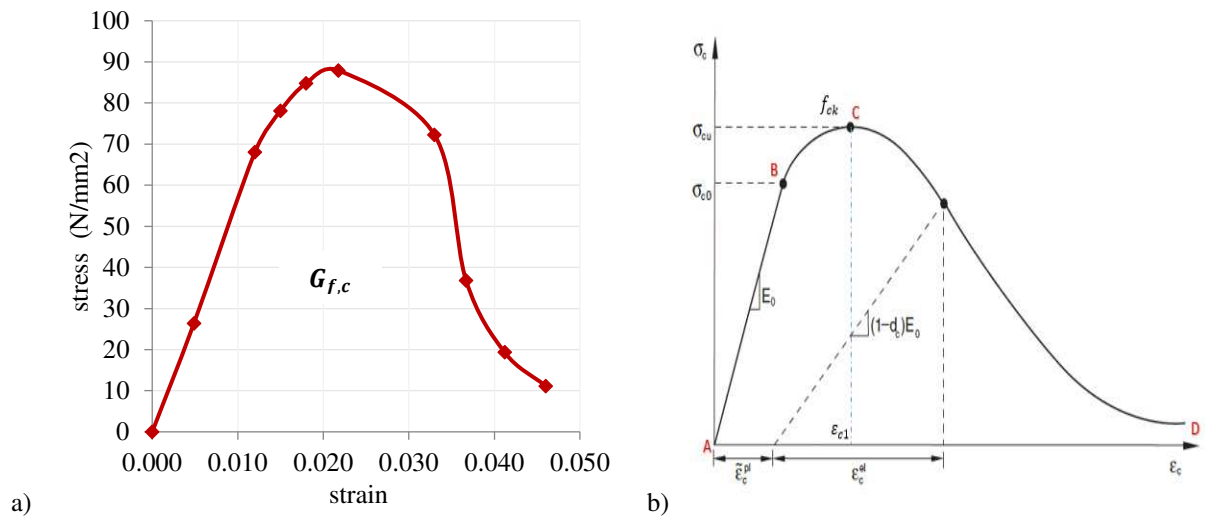
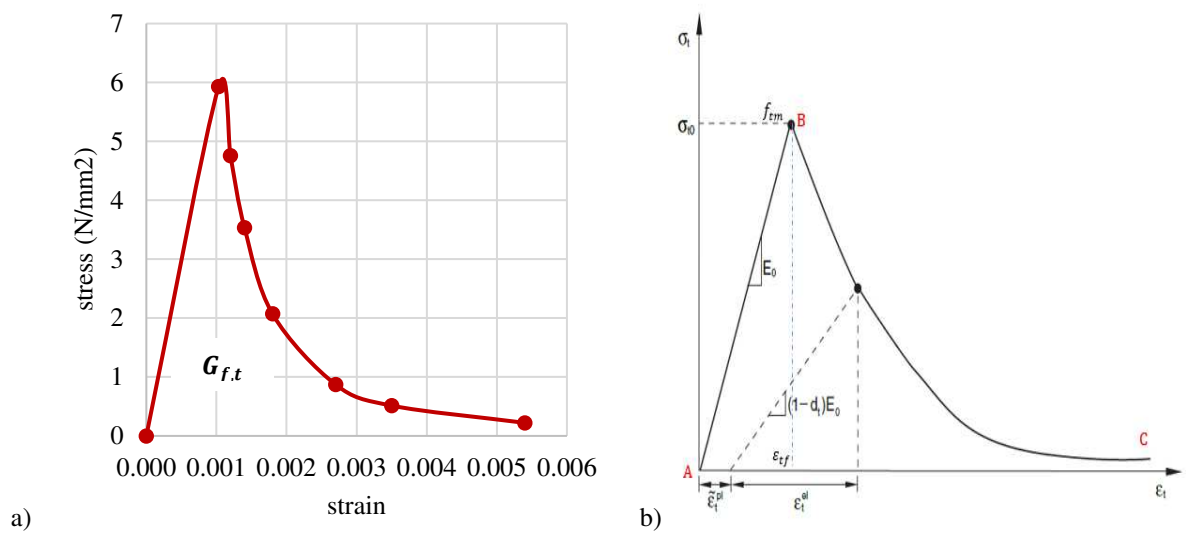Figure 8: Masonry unit behaviour under uniaxial tension (a) numerical model (b) typical response in ABAQUS (Simulia, 2014).

a)

b)

Figure 9: Mortar behaviour under uniaxial compression (a) numerical model (b) typical response in BS EN 1992-1-2:2004.

a)   b)
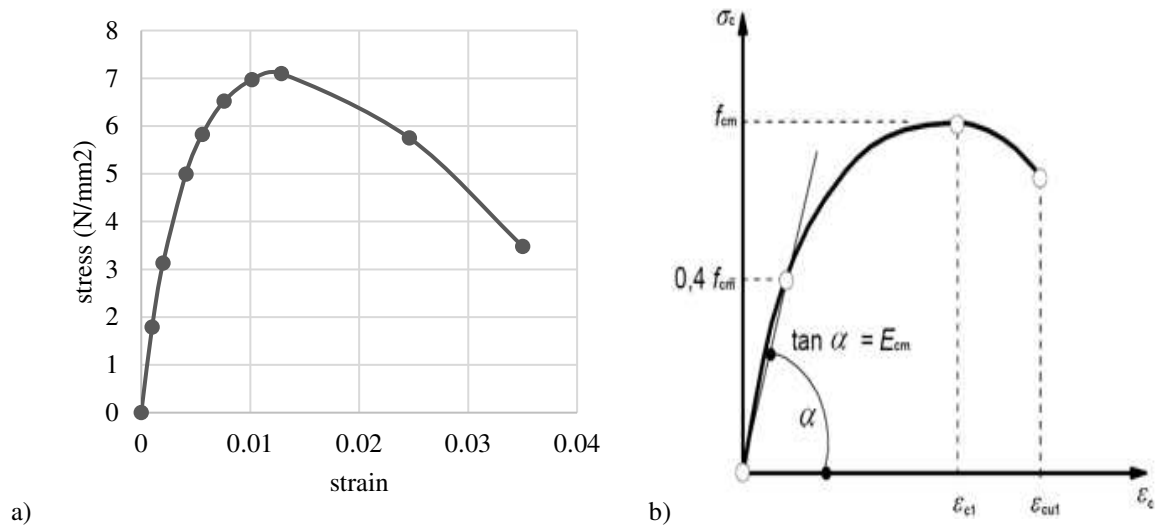
Figure 10: Mortar behaviour under uniaxial tension (a) numerical model (b) typical response in BS EN 1992-1-2:2004.

a)   b)
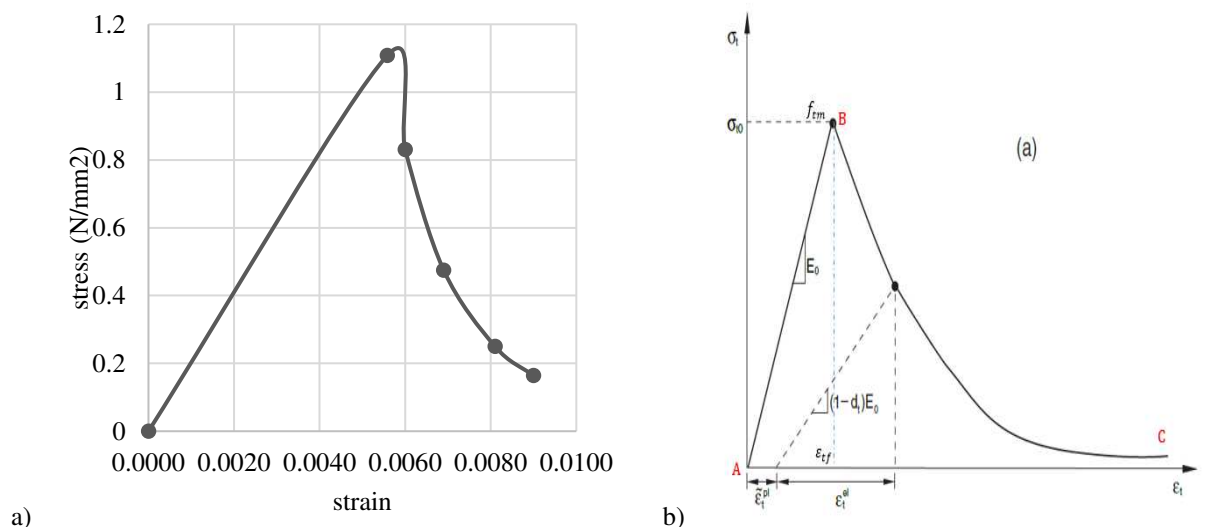
Figure 11: Friction behaviour (Simulia, 2014)
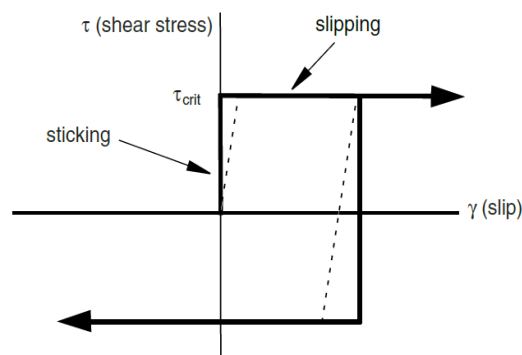
Figure 12: Tensile behaviour of present model vs. experimental results from Pluijm (1992)
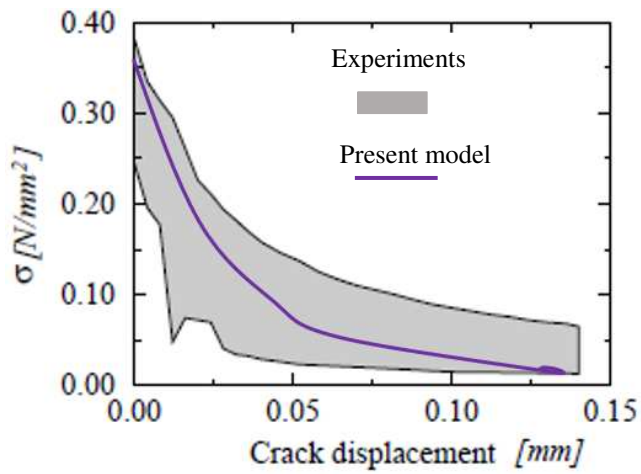
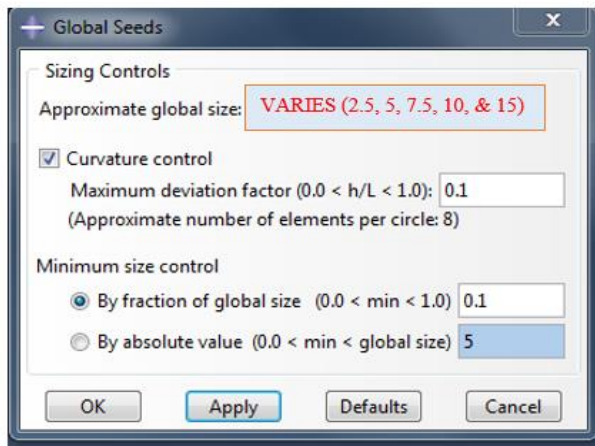Figure 13: Mesh seed global size control (Simulia, 2014)

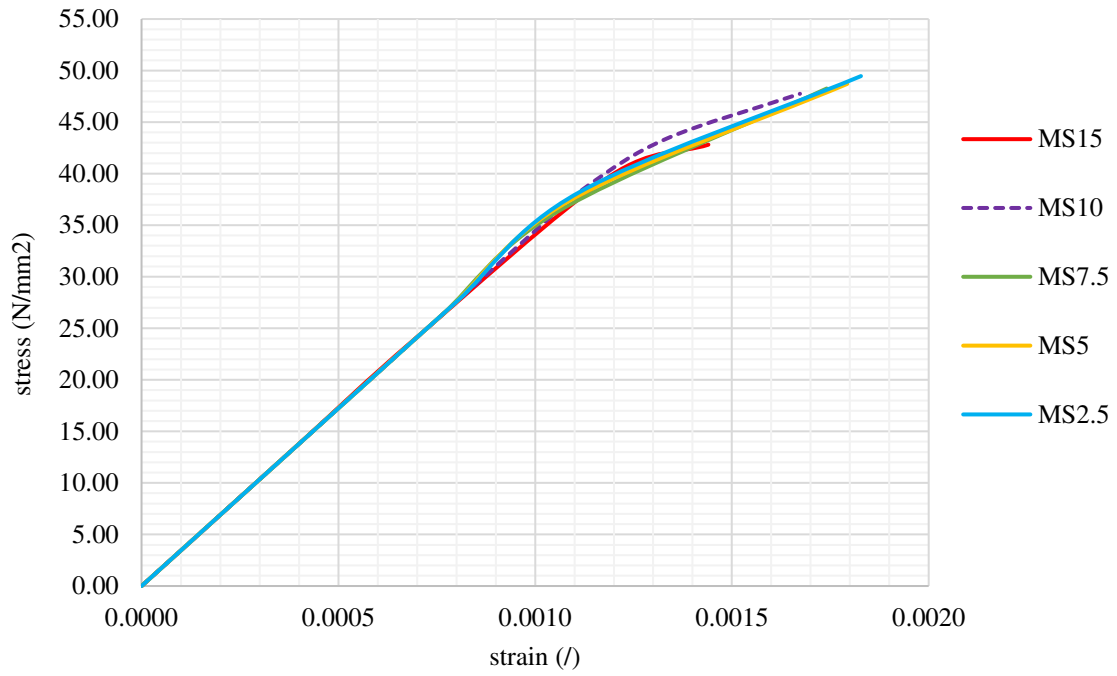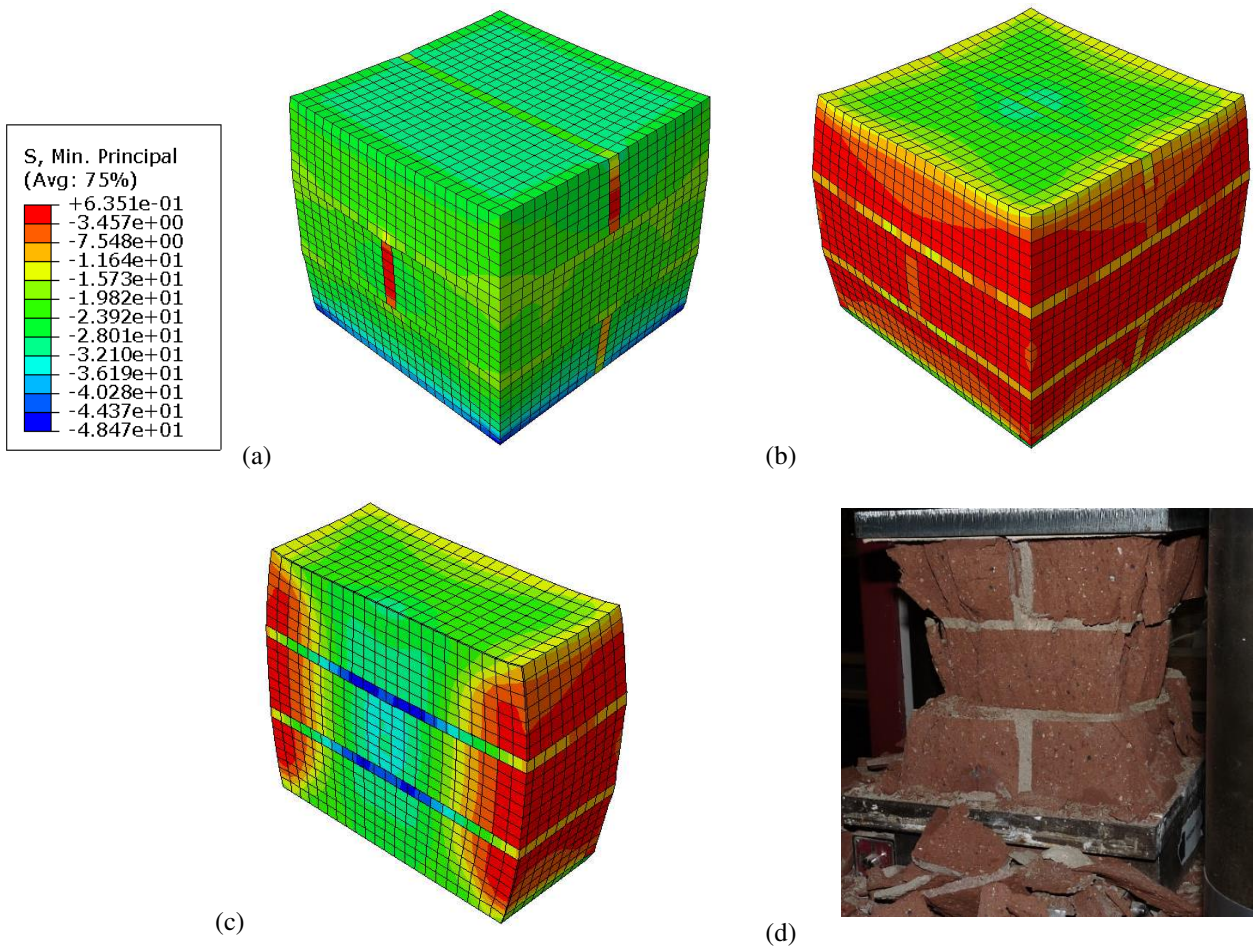Figure 14: Influence of mesh density on the numerical model

Figure 15: (a) minimum principal stress (b) maximum principal stress (c) view cut along y-plane to show stresses distribution in masonry cube (d) typical failure of specimen (e) compressive damage contour plot (f) tensile damage contour plot

S, Min. Principal
(Avg: 75%)
+6.351e-01
-3.457e+00
-7.548e+00
-1.164e+01
-1.573e+01
-1.982e+01
-2.392e+01
-2.801e+01
-3.210e+01
-3.619e+01
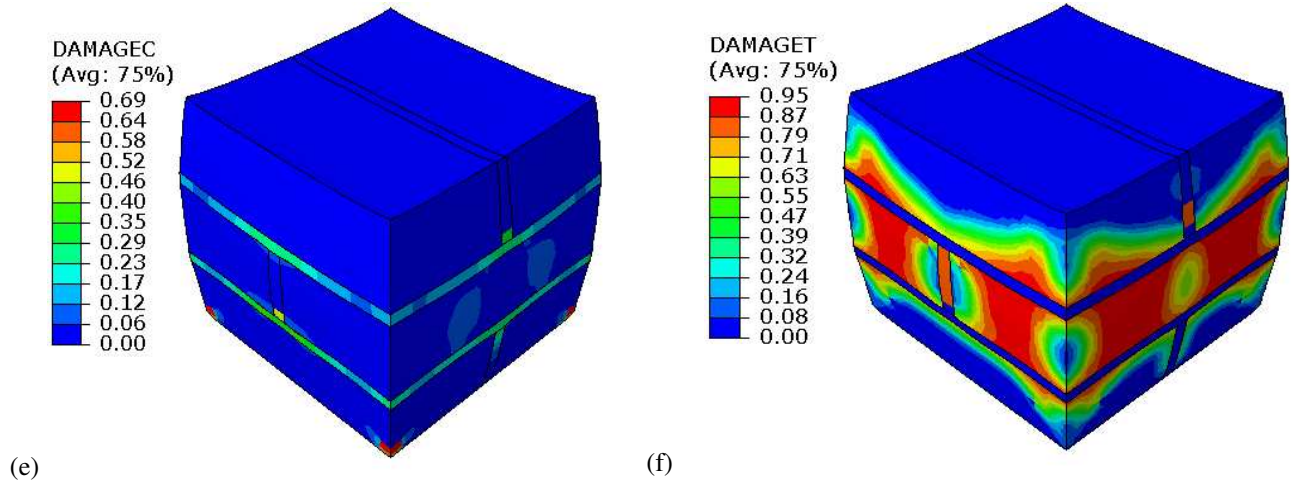-4.028e+01
-4.437e+01
-4.847e+01

(a)

(b)

(c)

(d)

(e)

(f)

Figure 16: Stress-strain curve of masonry cubic model